Cerebral Cortex, August 2017;27: 4244–4256

doi: 10.1093/cercor/bhx128
Advance Access Publication Date: 24 May 2017
Original Article

ORIGINAL ARTICLE

Relationship Between Synaptic AMPAR and Spine Dynamics: Impairments in the FXS Mouse

Anand Suresh and Anna Dunaevsky

Department of Developmental Neuroscience, Munroe-Meyer Institute, University of Nebraska Medical Center, 985960 Nebraska Medical Center, Omaha, NE 68198-5960, USA

Address correspondence to Anna Dunaevsky. Email: adunaevsky@unmc.edu

Abstract

Structural dynamics of dendritic spines are important for memory and learning and are impaired in neurodevelopmental disorders such as fragile X syndrome. Spine dynamics are regulated by activity-dependent mechanisms that involve modulation of AMPA receptors (AMPAR); however, the relationship between AMPAR and spine dynamics in vivo and how these are altered in FXS mouse model is not known. Here, we tracked AMPAR and spines over multiple days in vivo in the cortex and found that dendritic spines in the fmr1 KO mouse were denser, smaller, had higher turnover rates and contained less sGluA2 compared to littermate controls. Although, KO spines maintained the relationship between AMPAR and spine stability, AMPAR levels in the KO were more dynamic with larger proportion of spines showing multiple dynamic events of AMPAR. Directional changes in sGluA2 were also observed in newly formed and eliminated spines, with KO spines displaying greater loss of AMPAR before elimination. Thus, we demonstrate that AMPAR levels within spines not are only continuously dynamic, but are also predictive of spine behavior, with impairments observed in the fmr1 KO mice.

Key words: AMPAR, dendritic spines, fragile X, GluA2, motor cortex, multiphoton

Introduction

Dendritic spines are the principal sites of excitatory synapses in the neurons of mammalian central nervous system (Cajal 1888; Gray 1959). Spines are plastic and undergo structural and functional changes under basal and experience dependent conditions (Holtmaat et al. 2009; Fu and Zuo 2011). Structural dynamics involves spine formation and elimination as well as change in size of the spine (Dunaevsky et al. 1999; Trachtenberg et al. 2002; Alvarez and Sabatini 2007; Bosch and Hayashi 2012). The structural reorganization of dendritic spines is thought to be associated with synaptic plasticity mechanisms that involve modulation of synaptic strength via insertion or removal of α-amino-3-hydroxy-5-methyl-4-isoxazolepropionic acid receptor (AMPAR) (Malenka and Bear 2004; Turrigiano 2012; Chater and Goda 2014). Indeed, under in vitro conditions, both long-term potentiation (LTP) (Engert and Bonhoeffer 1999) and long-term depression (LTD) (Hasegawa et al. 2015) paradigms of synaptic plasticity have shown to induce spine formation and elimination, respectively. These changes are thought to bring about functional reorganization of the neuronal circuits and are critical for learning and memory (Hofer and Bonhoeffer 2010; Hayashi-Takagi et al. 2015). Although short-term activity-dependent changes in AMPAR in spines have been examined (Zhang et al. 2015), the link between synaptic stabilization over days and AMPAR insertion has not been previously studied in vivo.

Dendritic spines are altered in number of neurodevelopmental disorders (Penzes et al. 2011) including the fragile X syndrome (FXS), which is the most common inherited form of intellectual disability (Penagarikano et al. 2007). Moreover, in a mouse model of FXS, there is impaired structural and functional plasticity with increased spine turnover, reduced LTP and impaired experience dependent plasticity of spines (Cruz-Martin et al. 2010;

Pan et al. 2010; Padmashri et al. 2013; Contractor et al. 2015). Here, we therefore also investigated the relationship between AMPAR insertion and dendritic spine dynamics in an FXS mouse model.

To investigate the role of AMPAR in spine fate and dynamics in vivo, we expressed AMPAR subunit GluA2 tagged to super-ecliptic phluorin (SEP), a pH sensitive GFP variant (Miesenbock et al. 1998), in layer 2/3 neurons of the primary motor cortex (M1). Since the majority of AMPAR contain the GluA2 subunit (Lu et al. 2009), we used SEP-GluA2 (sGluA2) levels in spines as a proxy for synaptic AMPAR. Dendritic spines and sGluA2 were imaged in vivo using two-photon microscopy over a period of 10 days in wild type mice and in the FXS mouse model, the fmr1 knock out (KO) mice. Repeated in vivo imaging revealed that in the fmr1 KO mouse dendritic spines were denser, smaller, contained less sGluA2 and had higher turnover rates (TORs) compared to littermate controls (WT). Our data confirmed the relationship between synaptic strength and synaptic stability, with greater AMPAR containing spines being more stable in both WT and the KO mice. Additionally, we observed that AMPAR levels were dynamic in most stable spines, fluctuating over 10 days with larger proportion of spines showing multiple dynamic events of AMPAR in the KO. Directional changes in sGluA2 were also observed in subpopulation of spines, with new small spines gradually accumulating sGluA2. Finally, sGluA2 levels dropped just prior to spine elimination with greater loss observed in the KO spines. Thus, we conclude that AMPAR levels within spines are continuously dynamic but are also predictive of spine behavior, with impairments observed in the fmr1 KO mice.

Materials and Methods

Mice

Mice were cared for in accordance with NIH guidelines for laboratory animal welfare. All experiments were approved by the University of Nebraska Medical Center Institutional Animal Care and Use Committee. Female C57BL/6 fmr1 heterozygous (HET) mice were crossed with male C57BL/6 fmr1 KO mice and used for in utero electroporation. Since FXS predominantly affects boys, male WT littermates and fmr1 KO pups were used for all experiments.

DNA constructs: we used a FUGW pUB-SEP-GluA2-WPRE and pCAG-tdTom constructs for our experiments. FUGW pUB-SEP-GluA2-WPRE was a generous gift from the lab of Noam Ziv (Zeidan and Ziv 2012). First, SEP, a pH sensitive GFP variant (Miesenbock et al. 1998) was tagged to the N terminus of GluA2, and the SEP-GluA2 (sGluA2) was cloned under the ubiquitin promoter in a FUGW lentiviral construct. For the morphological tracer, we used pCAG-tdTomato construct where the tdTomato (tdTom) was cloned under a CAG promoter.

In utero Electroporation

Timed pregnant female C57BL/6 fmr1 HET mice were in utero electroporated as described previously (Fig. 1*b*) (Saito and Nakatsuji 2001). Briefly, embryonic (E) day 15.5 timed pregnant C57BL/6 fmr1 HET mice were anaesthetized using an isoflurane-oxygen mixture (induction: 5% Isoflurane/2 liter/min O2, maintenance: 2% isoflurane/2 liter/min O2). A small incision was made within the abdominal walls and uterine horns were exposed. A 0.5 μL of 4 μg/μL DNA solution of pCAG-tdTomato and pUB-SEP-GluA2-WPRE was injected into the cerebral ventricles of E15.5 mouse embryo using Parker Picospritzer III microinjection system. The head was then placed between tweezer electrodes so as to target the motor cortex. Electroporation was achieved using 5 square pulses (5 ms long at 1 Hz, 35 mV). Embryos were returned back into the abdominal cavity and dams were revived and allowed to deliver normally.

Tissue Preparation and Immunohistochemistry

Mice were perfused with 4% paraformaldehyde at postnatal day 30, and brain sections (100 μm) containing the primary motor cortex were selected for analysis. Sections were incubated in 10% normal goat serum (NGS) and 0.3% Triton X-100 for 3 min, then washed 3 times with PBS, preincubated for 1 h in 5% NGS and then immunostained with primary antibodies against GluA2 (polyclonal 1:500, Millipore MAB397) overnight at 4 °C. The secondary antibody was Alexa 647 coupled antiguinea pig (1:500, Invitrogen), in 1% NGS and 0.3% Triton X-100, for 90 min at RT.

Cranial Window

At postnatal day, 28–30 mice were anesthetized with Tribromoethanol (Avertin, 0.25 mg/g body weight) and a cranial window was implanted over the motor cortex (Fig. 1*c*). Briefly, half an hour before the surgery, dexamethasone (~2 μg/g body weight) and carprofen (5 μg/g body weight) were injected intraperitoneally to reduce cerebral edema and inflammation during the craniotomy. A 5 mm craniotomy centered on bregma, was made across the sutures, above the primary motor cortex. After the craniotomy, the exposed surgery site was rinsed with an enrofloxacin antibiotic solution (0.5 μg/mL) and covered with a 5-mm diameter cover glass, which was permanently glued to the skull using dental acrylic cement. The dura remained intact in this procedure. Mice were treated with antibiotic enrofloxacin (5 mg/kg) twice daily for 6 days after surgery to prevent bacterial infection. Mice were also injected daily with carprofen (5 mg/kg) for 3 weeks following surgery to reduce inflammation. Mice were allowed 3 weeks to recover from the surgery.

Imaging

All imaging was performed with a multiphoton microscope (Moving Objective Microscope, MOM; Sutter), using a Ti: Sapphire laser (Chameleon Vision II, Coherent) tuned to 925 nm. Mice were anaesthetized with a ketamine/dexdormitor mixture (100 and 0.5 mg/mL, respectively, 2.5 mL/kg). Images were collected with a Nikon water-immersion objective (60X, 1.0 NA). Excitation power measured at the back aperture of the objective was typically ~20 mW and was adjusted to achieve near identical levels of fluorescence for each imaged region using a Pockel cell. Two-channel imaging was achieved by using a 565 nm dichroic mirror and 2 external photomultiplier tubes. A 535/50 bandpass filter was used to detect sGluA2 emission and a 610/75 bandpass filter was used to detect tdTom. For imaging, we used ScanImage software written in MATLAB (MathWorks) (Pologruto et al. 2003). During an imaging session, 6 to 10 regions of interest (ROIs) per animal were selected along the dendritic tufts of tdTom and sGluA2 expressing layer 2/3 pyramidal neurons (Fig. 1*d*). All imaged dendrites were in layer 1 (within the first 100 μm below the dura matter) within the forelimb M1, as determined by stereotaxic measurements (between 750 and 2000 μm lateral to the midline and between 1000 μm rostral and 250 μm caudal from bregma) (Tennant et al. 2011). Each ROI consisted of a stack of images (20–80 optical sections, separated axially by 1 μm). The coordinates of each ROI were recorded using the XYZ motor on the MOM for subsequent imaging days. After imaging,

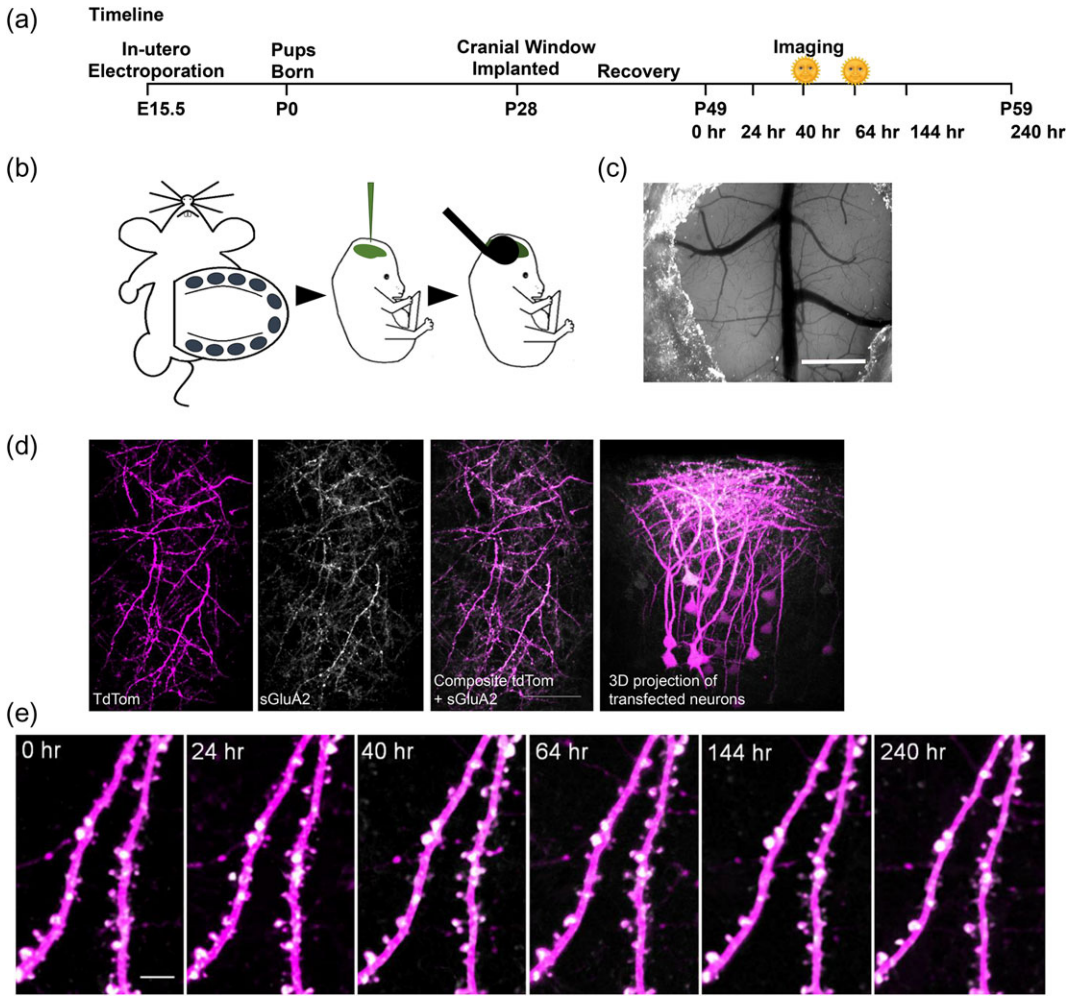

Figure 1. Repeated in vivo imaging of doubly transfected layer 2/3 neurons of M1 cortex. (*a*) Experimental time course. Morning sessions are marked with a symbol. (*b*) Embryos from E15.5 timed pregnant C57Bl6 fmr1 HET mice were injected with a mixture of pUB-SEP-GluA2-WPRE and pCAG-tdTom DNA constructs into the lateral ventricles and neurons were transfected using an electrode tweezer. (*c*) A cranial glass window implanted over the motor cortex. Scale bar: 1 mm. (*d*) 2PLSM in vivo images of transfected region of cortex showing overlap of tdTom (magenta) and sGluA2 (white) along with 3D projection of a Z of the same region. Scale bar: 100 μm. (*e*) Repeated in vivo imaging of apical dendrites of layer 2/3 neurons in M1 cortex showing stable expression of tdTom and sGluA2 over the experimental duration. Scale bar: 5 μm.

mice were revived from anesthesia with Antisedan (atipamezole hydrochloride 5.0 mg/mL). Images were collected 6 times over a period of 10 days at intervals indicated in Figure 1. Imaging was performed at 5PM for all days except for the 40 and 64 h session where images were collected at 9AM.

Image Analysis

Spine Identification

All images were corrected for tdTom bleed-through into sGluA2 (green) channel by quantifying percent bleed-through on a tdTom only expressing mouse and subsequently subtracting out the bleed-through from images of the sGluA2 (green) channel images. A custom written imaging program written in python was used to track dendritic spines and sGluA2 levels over imaging sessions. Dendritic segments of 30–80 μm were chosen in 3D stacks and dendritic spines were identified and marked in tdTom image channel on 0 h images (Figure S1a). Unless mentioned otherwise, 0 h images were considered as baseline for all analysis. For spine dynamics, images were compared to baseline images and categorized as stable if they were present in both images, eliminated if they appeared in the previous image but not in the image being analyzed and newly formed when they appeared in the image being analyzed but not in the baseline image. Spine formation and elimination was calculated as a percentage of new or eliminated spines of the total number of spines at baseline. TORs were calculated as ratio of sum of spines formed and eliminated to twice the total number at baseline (Holtmaat et al. 2005).

sGluA2 and Spine Intensity Measurement

To mark a spine, an ROI was placed manually over the spine with care being taken not to include the dendrite (Figure S1a). To correct for background, a similar sized ROI was placed adjacent to the spine but away from the dendrite. To normalize across imaging sessions, we used tdTom dendrite intensity values, as these were relatively stable across sessions (Figure S1b-d). For normalization, two 16 pixel rectangular ROI were marked on either side of the spine, and average dendritic shaft tdTom value was measured and a normalization factor derived by comparing the tdTom dendrite values to baseline (Day 0 of imaging) values. Care was taken to place the dendrite ROI on a stretch of dendrite

that did not have a spine protruding in the z plane. To quantify sGluA2 and spine intensity, the sum of total integrated pixel intensity within the spine ROI across the 3 brightest optical frames of the spine was calculated for each channel, individually corrected for background and normalized to Day 0 unless otherwise stated. Since spine brightness is correlated with spine volume, we used spine intensity as a measure of spine size (Holtmaat et al. 2005, 2009). Spines were reidentified on subsequent sessions and intensity values measured as above. For new spines appearing during imaging sessions, spines were marked and sGluA2 and spine intensity were quantified and normalized to time of identification, except in Figure S4a where normalization was performed to Day 0. For Figure S4a, a mean dendrite ROI value was calculated for each dendrite for Day 0 and Day 10 to obtain a normalization factor that was then applied for all spines. For presentation purposes, all images were de-speckled and smoothened. Crisscrossing axons traversing the field of view were removed from some frames and 3–5 frames were maximally projected. All analysis was done blinded to mouse genotype on unprocessed images except for the bleed-through correction described above. For all analysis, unless indicated otherwise, the averages were calculated per mouse.

Percentile Spine Grouping

sGluA2 intensity for all spines within a dendrite (30–80 μm) at baseline was arranged in an ascending order and percentile rank for every spine calculated. Spines were divided into 4 percentile groups (bin width of 25) with progressively increasing levels of sGluA2. Within each mouse, the fraction of stable spines (Fig. 3*b*) and sGluA2 percentage changes (Fig. 4*f*) were quantified. For Figure S3a, we calculated the average sGluA2 intensity per dendrite for each percentile group in the WT and applied the intensity values as cutoffs to the KO dendrites. For the *k*-means cluster analysis we used a 2-partition *k*-means test on MATLAB to separate out High and Low sGluA2 containing spines per dendrite. Fraction of stable spines per group and proportion of clusters per genotype were calculated (Figure S3c-d).

Local Dendrite Ranking

Similar sGluA2 intensity spines ("target spines," minimally 10 μm apart) with opposing fates were identified on a baseline image. sGluA2 within spines in 5-μm stretches on either side of the target spine (cluster) was quantified and arranged in an ascending order. These were then ranked in steps calculated by 10/(total number of spines in a cluster − 1) with the smallest spine given a rank of zero, the next spine a rank of zero + step size and with the largest a rank of 10. In Figure 3c, for representation purposes only, the ranking is represented as whole numbers with the largest sGluA2 containing spines getting rank of *n* (which is total number of spines per cluster) and the smallest a rank of 1.

New Spines Grouping

For both genotypes, spines within dendrites imaged at 40 and 64 h were pooled for further analysis (Figure S5d for proportion of spines per imaging interval). Dendritic rank of new spines (Figure S5b) and fraction of stable spines (Figure S5c) per sGluA2 level groups of all newly formed spines within these sessions were calculated per dendrite and averaged per mouse similar to the method used in persistent spines and compared across groups and genotypes.

sGluA2 Spine Dynamic Grouping

sGluA2 dynamics was quantified as percentage change of sGluA2 at all time points compared to the previous time point. We defined change as ±2 SD of the percentage change at 24 h in WT which sets a threshold of ±30% (Zhang et al. 2015). Spines were classified as "no change" if sGluA2 intensity did not cross the threshold on all days and "dynamic" if they did. Additionally, we monitored the direction of changes (increases or decreases) at all time points for all spines and specifically calculated proportion of spines per mouse showing multiple changes in direction of sGluA2 percentage changes. We used the coefficient of variation (CV) function on excel to calculate CV for every individual spines per mouse.

Statistics

Analysis was done on GraphPad prism and error bars represent standard error means (SEMs). To test for statistical significance an unpaired Student's *t*-test (Figs 2*a*, 4*d*), multiple *t*-test with post hoc Bonferroni correction (Fig. 2*b–d*), one-way ANOVA with post hoc Bonferroni correction (Fig. 4*g*), two-way ANOVA with post hoc Bonferroni correction (Figs 3*b*,*d*, 4*c*, 5*c*, 6*d*), two-way repeated ANOVA with post hoc Bonferroni correction (Fig. 4*e*), Kolmogorov–Smirnov test (Fig. 2*e*, *f*).

Results

Repeated In Vivo Imaging of Dendritic Spines and SEP-GluA2

To track spine and AMPAR dynamics in layer 2/3 pyramidal neurons of M1 cortex, E15.5 mouse embryos were in utero electroporated with AMPAR subunit GluA2 tagged to superecliptic phluorin (sGluA2) and morphological tracer td-Tomato (tdTom) (Fig. 1). For repeated in vivo imaging, a cranial window (Holtmaat et al. 2009) was implanted over the primary motor cortex (M1 cortex) using previously published coordinates (Fig. 1c) (Tennant et al. 2011). Following recovery, mice were imaged and dendrites expressing bright signal across both channels were chosen for imaging (Fig. 1*d*). Stable images were obtained over a 10-day period with no evidence of photobleaching (Fig. 1*e* and Figure S1b&d). While tdTom had uniform expression throughout the cells, sGluA2 had a punctate appearance with relatively low expression in the dendritic shaft and negligible expression within axons, as would be expected from a postsynaptic protein (Fig. 1*e*, S2a) (Zhang et al. 2015). Moreover, sGluA2 expression was detected even within immature filopodia-like structures (Zito et al. 2009) giving us further confidence in our ability to track AMPAR in vivo (Figure S2b). The use of sGluA2 tagged to SEP, allowed the tracking of only surface bound GluA2 which are the functionally relevant pools of AMPAR (Kopec et al. 2006). Immunostaining of sections from transfected mouse brains with an antibody against GluA2 indicated about a 50% overexpression of sGluA2 at postnatal day 30 (Figure S1c). To test whether sGluA2 overexpression affected spine morphogenesis and dynamics, we compared spine density in layer 1 apical dendrites of layer 2/3 neurons of WT mice transfected with sGluA2/tdTom to WT mice transfected with tdTom alone (Figure S2d). We observed no difference in spine density between the groups (WT sGluA2/tdTom: 0.69 ± 0.01spines/μm $n = 5$ mice, WT tdTom: 0.68 ± 0.02 spines/μm, $n = 3$ mice, $P > 0.05$). Similarly, spine dynamics was also not altered with overexpression of sGluA2 compared to previous reports (6% formation and elimination over 24 h) (Ma et al. 2016) (Fig. 2*b–d*). Thus with the in utero electroporation and cranial window strategy,

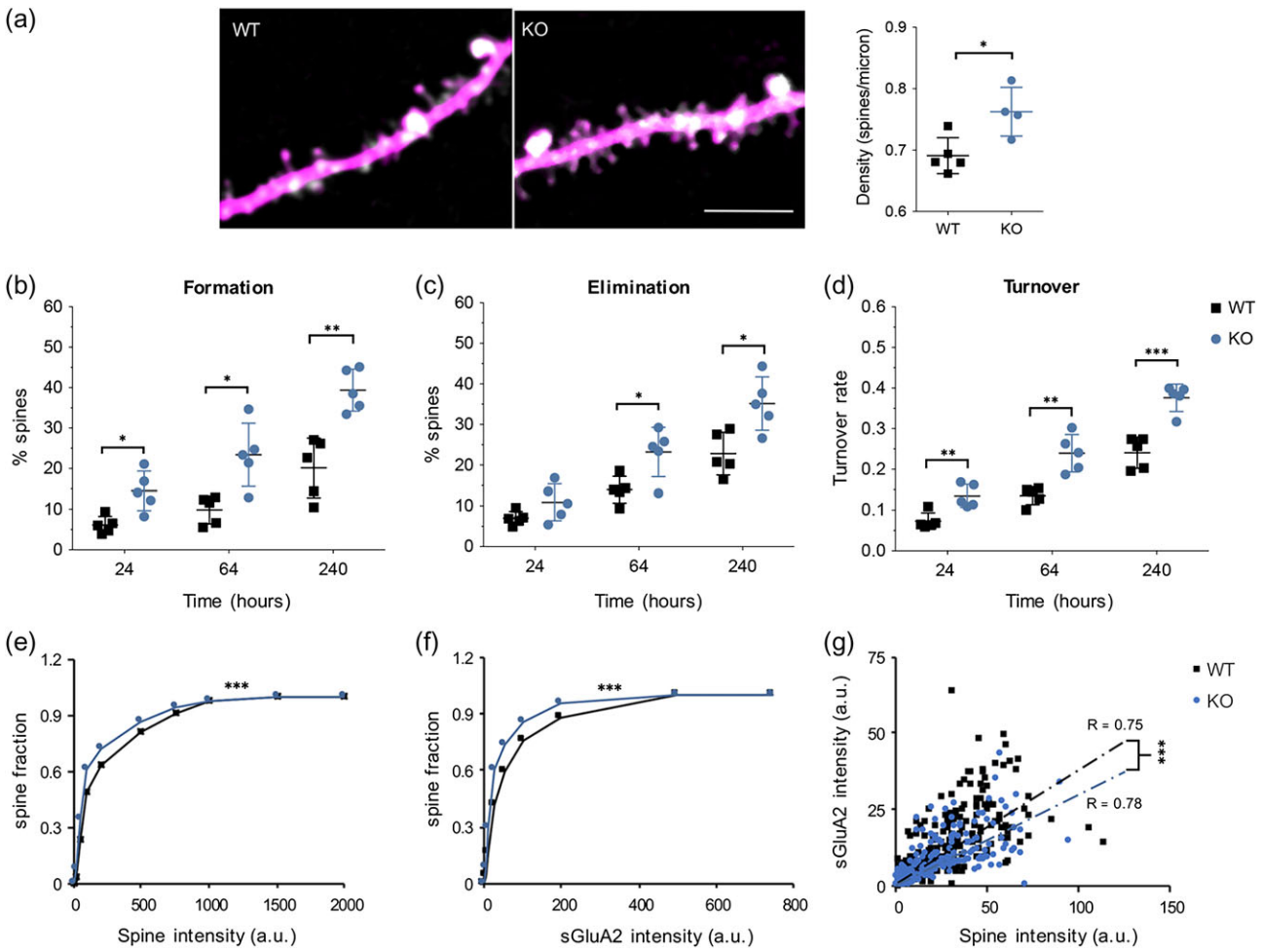

Figure 2. Altered dendritic spine properties and spine size in the fmr1 KO mice. (*a*) Representative images of dendrites from layer 2/3 pyramidal neurons expressing tdTomato and sGluA2 in WT and KO mice. Spine densities were significantly higher in the KO mice (WT: 0.69 ± 0.01 spines/μm, KO: 0.76 ± 0.02 spines/μm, $n = 5$ mice, unpaired *t*-test, $^{*}P < 0.05$) Scale bar: 10 μm. (*b*) KO mice had increased spine formation over short, intermediate and long time intervals (24 h: WT 6.121 ± 0.5%, KO 14.5 ± 2.17%, 64 h: WT 9.834 ± 1.53%, KO: 23.41 ± 3.5%, 240 h: WT 20.16 ± 3.3%, KO: 39.38 ± 2.3%, $n = 5$ mice, multiple *t*-test with Bonferroni–Sidak correction, $^{*}P < 0.05$, $^{**}P < 0.01$). (*c*) KO mice had increased spine elimination over intermediate and long time intervals but not over short intervals (24 h: WT 6.99 ± 0.75%, KO 10.9 ± 2.03%, 64 h: WT 13.96 ± 1.46%, KO 23.22 ± 2.71%, 240 h: WT 22.81 ± 2.35%, KO 35.15 ± 3.9%, $n = 5$ mice, multiple *t*-test with Bonferroni–Sidak correction, $^{*}P < 0.05$). (*d*) TORs were elevated in the fmr1 KO mice (24 h: WT 0.07 ± 0.01, KO 0.14 ± 0.01, 64 h: WT 0.135 ± 0.01, KO 0.24 ± 0.02, 240 h: WT 0.24 ± 0.02, KO 0.38 ± 0.01, $n = 5$ mice, multiple *t*-test with Bonferroni–Sidak correction, respectively, $^{**}P < 0.01$, $^{***}P < 0.001$). All data represented as mean ± SEM. (*e*, *f*) Cumulative frequency plots of spine intensity and sGluA2 intensity at 0 h. Spine and sGluA2 intensities were smaller in the fmr1 KO mice compared to WT mice (WT: $n = 480$ spines, KO: $n = 478$ spines, Kolmogorov–Smirnov test, $P < 0.001$ for both spine intensity and sGluA2 intensity). (*g*) Linear correlation between spine intensity and sGluA2 in WT and KO mice (WT: $R = 0.75$, $n = 480$ spines, KO: $R = 0.78$, $n = 470$ spines, $^{***}P < 0.001$). The slope of the KO linear regression was significantly lower (WT slope: 3.74 ± 0.12, $n = 480$ spines, KO slope: 3.03 ± 0.14, $n = 478$ spines, fixed effect regression analysis, $^{***}P < 0.001$).

we were able to repeatedly image and track both dendritic spines and spine AMPAR in apical dendrites of layer 2/3 pyramidal neurons of the motor cortex over multiple days.

Altered Spine Density, Size, and Dynamics in the Primary Motor Cortex of fmr1 KO Mice

Reports of altered dendritic spine density and dynamics in the KO mice have been variable with spine properties depending on brain region, age and layer of neurons investigated (He and Portera-Cailliau 2013). As no previous studies had investigated spine properties in layer 2/3 pyramidal neurons in the M1 cortex at 8 weeks of age, we first investigated spine density (Fig. 2*a*). Unlike in layer 5 neurons (Padmashri et al. 2013), we observed an 11% increase in dendritic spine density of layer 2/3 pyramidal neurons in the KO mice as compared to tdTom/sGluA2 expressing WT mice (Fig. 2*a*, $P = 0.017$). To investigate spine dynamics in layer 2/3 neurons of M1, we quantified spine formation and elimination over short (24 h), intermediate (60 h), and long (240 h) durations and compared across genotypes. We observed higher rates of formation at all intervals (Fig. 2*b*, $P \leq 0.02$ for all comparisons) but increased elimination only at intermediate and longer time points (Fig. 2*c*, 64 h: $P = 0.049$, 240 h: $P = 0.03$). This increased formation and elimination also translated to higher TORs calculated at all intervals (Fig. 2*d*, 24 h: $P = 0.01$, 64 h: $P = 0.006$ and 240 h: $P = 0.001$). Thus, our data suggest that at 2 months, KO mice have increased spine densities and higher rates of spine dynamics in apical dendrites of layer 2/3 pyramidal neurons in the M1 cortex.

Reports from humans with FXS (Hinton et al. 1991; Irwin et al. 2001) and fmr1 KO mice (He and Portera-Cailliau 2013) have described preponderance of small immature looking

spines. We observed a significant shift in the distribution of both sGluA2 intensity and spine intensity ($P < 0.001$), which is an approximation of spine volume (Holtmaat et al. 2005), suggesting smaller spines in layer 2/3 neurons in the KO (Fig. 2*d*, *e*). This was not due to differences in tdTom expression since mean dendrite intensity values were similar across WT and KO (Figure S1c, $P > 0.5$). Spine size and AMPAR levels are known to be strongly correlated (Noguchi et al. 2011; Zhang et al. 2015) and we observed the same in the WT (Pearson $r = 0.75$, $P < 0.001$). Although these correlations were similar in the KO (Pearson $r = 0.78$, $P < 0.001$), surprisingly the slope of sGluA2 versus spine intensity linear regression line was smaller compared to the WT (Fig. 2*f*, $P < 0.0001$). This suggests altered structure function relationship in the KO with less sGluA2 per spine. Altogether, our results suggest a larger pool of small spines in layer 2/3 pyramidal neurons and altered AMPAR-spine size correlation in the M1 cortex of the fmr1 KO mice.

Spine Fates and AMPAR Levels

Strength of synaptic transmission at an excitatory synapse is mediated by the levels of AMPA receptors within the synapse (Matsuzaki et al. 2004). Large synapses have been shown to have stronger synaptic transmission and to be more stable (Matsuzaki et al. 2004; Holtmaat and Svoboda 2009). Yet, the direct relationship between levels of AMPAR and spine stability has not been investigated in vivo. We therefore next investigated whether sGluA2 levels within a spine correlated with spine fates and whether this relationship was altered in the KO mice. A total of 640 and 680 spines were quantified from 19 and 20 dendrites from 4 mice in WT and KO, respectively, over a period of 10 days measuring synaptic sGluA2 levels, spine intensity levels and noting spine fate. We ranked spines based on sGluA2 levels at Day 0 and divided them into 4 equal sized groups with increasing levels of sGluA2 (Fig. 3*a*, see Methods). Proportion of stable versus eliminated spines per group was then determined for every mouse and compared across genotypes.

We found that in the WT mice the stability of dendritic spines increased progressively with increasing levels of sGluA2 (Fig. 3*b*). Thus, the spines with lowest amounts of sGluA2 (Group 1) had average stability of 38% whereas spines with the highest amount of sGluA2 (Group 4) were all stable. The remaining spines in Groups 2 and 3 had intermediary spine stability of 76% and 92%, respectively. Although the trend of increased spine stability with higher sGluA2 levels was maintained in the KO, this relationship was altered with approximately 22% and 20% reduction in stability within Groups 2 and 3, respectively (WT vs. KO $P = 0.002$ and $P < 0.001$, respectively) but no difference in the groups with the lowest and highest sGluA2 levels. Since, there is a greater proportion of low sGluA2 containing spines in the KO which could then spillover into higher groups and lower their overall stability, we regrouped the KO spines by sGluA2 cutoffs of the WT and observed similar stability levels between the genotypes (Figure S3a&b, $P > 0.5$). Similar results were also obtained when the data were clustered into High and Low sGluA2 groups, using a *k*-means partition analysis (Figure S3c). Spines of the High sGluA2 group were highly stable while spines of the Low sGluA2 had decreased stability. Interestingly, in the KO the proportion of spines with high levels of sGluA2 was significantly smaller which is consistent with the finding of a larger population of smaller spines in the KO (Figure S3d).

Although spines with more sGluA2 are generally more stable we observed many spines with very similar levels of sGluA2 showing opposite fates in both WT and KO dendrites. Since spines are not uniformly distributed along the dendrite and local synaptic activity (Oh et al. 2015) and synaptic competition (Fonseca et al. 2006) for resources are linked to shaping structural changes we hypothesized that the local ranking of a spine within its immediate vicinity would be a stronger determinant of spine fate than global dendrite ranking. To test this hypothesis, across both genotypes, we identified spines of similar sGluA2 levels but opposing fates which were at least 10 μm apart (Fig. 3*c*). We then computed the rank of the target spine within the 10 μm dendrite stretch surrounding it. We quantified 120 spines from 22 dendrites and identified 62 stable (34 WT and 28 KO) and 58 eliminated (30 WT and 28 KO) spines. The properties of the clusters of eliminated and persisting target spines were similar; with no difference observed in number of spines per cluster, in target spine intensity and target spine sGluA2 intensity (Figure S3e-g). Yet, the average local rank of stable spines was significantly higher (93% in WT and 71% in KO) than those of the eliminated spines (Fig. 3*d*, $P < 0.001$). Our results suggest that local sGluA2 level rank and thus relative strength of synapses within their local environment influences spine stability.

sGluA2 Dynamics within Stable Spines

Synaptic transmission at dendritic spines is mediated through AMPAR. Although, synapses in the brain are continuously modified by experience, the dynamic properties of synaptic AMPAR levels over days in vivo are not known. To determine AMPAR dynamics, we identified stable spines (350 spines per genotype) and quantified sGluA2 and spine intensity. We observed that although total synaptic sGluA2 content within a dendrite did not vary over days (Figure S4a), sGluA2 levels within individual stable spines fluctuated from one imaging day to another in both WT and KO mice (Fig. 4*a*). We categorized spines based on sGluA2 intensity changes over 240 h (Fig. 4*b*,*c*, see Methods). Surprisingly, sGluA2 content in about 90% of spines in both WT and KO was dynamic (Fig. 4*c*, WT: $P < 0.001$, KO, $P < 0.001$). The changes were bidirectional with 40% of spines (data not shown) showing reversals in direction of change (increase followed by a decrease or vice versa) in both genotypes. Although a similar proportion of spines had at least one reversal of direction of sGluA2 change (data not shown), the proportion of spines exhibiting multiple fluctuations in direction of sGluA2 change over the 240 h period was 40% higher (Fig. 4*d*, WT 0.2 ± 0.02, KO 0.28 ± 0.02, $P = 0.04$), suggesting more dynamic sGluA2 in KO spines. A trend towards increased coefficient of variation of sGluA2 in the KO was also observed (Figure S4b, $P = 0.106$).

Despite these fluctuations, on average, stable spines in WT and KO had no changes in sGluA2 and tdTomato across all time points and genotypes when averaged by geometric means (Fig. 4*e*, Figure S4c). We calculated the geometric mean of spine changes per mouse since arithmetic means are biased towards positive increases given the high variability in sGluA2 changes. Interestingly, when we grouped spines based on initial levels of sGluA2 (Fig. 4*f*,*g* & Figure S4, see Methods) we found that spines with least sGluA2 had significantly larger increases in both WT and KO compared to spines with more sGluA2 (Fig. 4*g*, WT and KO, $P < 0.05$ for all comparisons).

Thus, we observed that majority of persistent spines had dynamic AMPAR levels. In the KO, a higher proportion of spines had multiple sGluA2 dynamic events as compared to the WT. On average, although the levels of sGluA2 did not change over time in either genotype, the least sGluA2 containing spines had

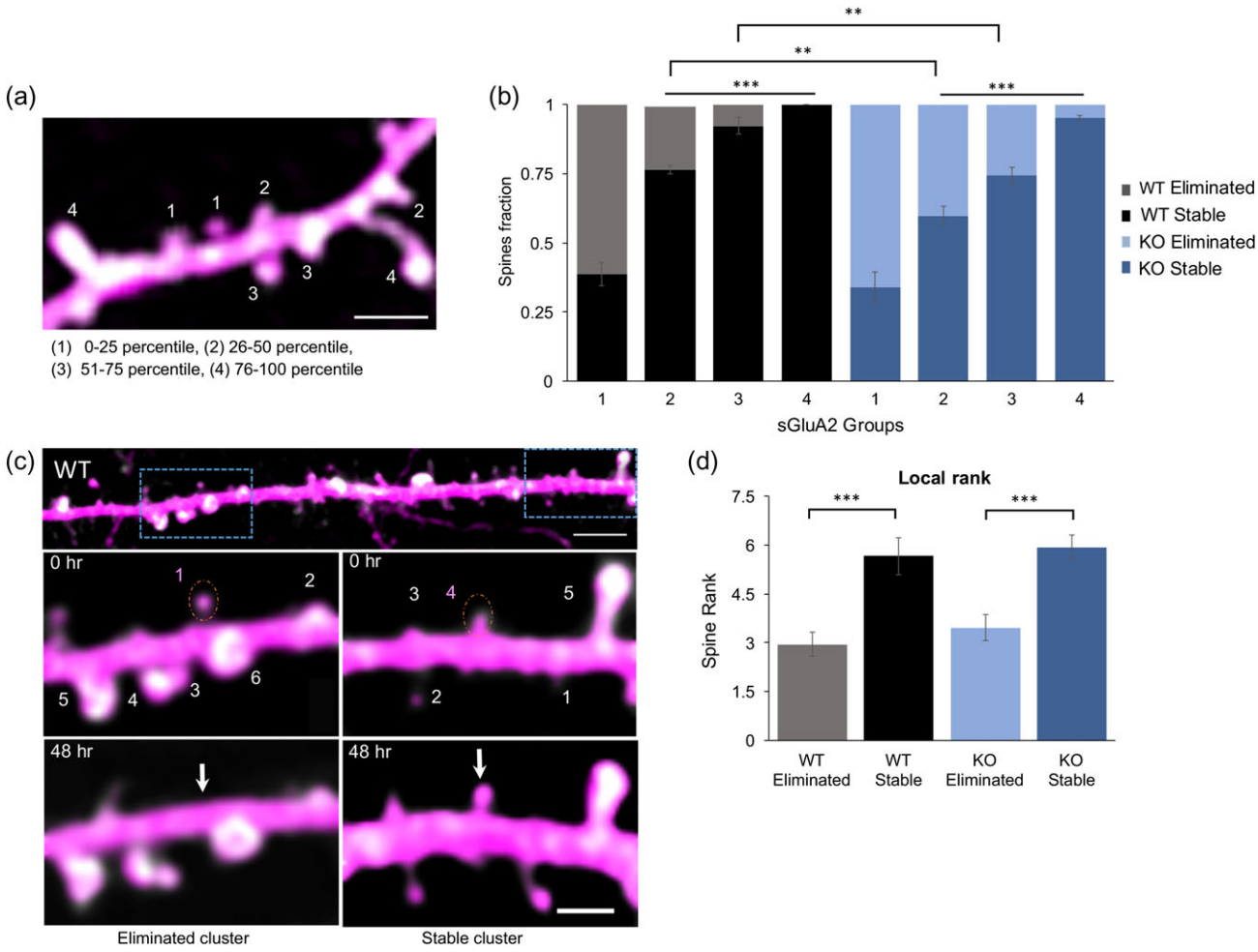

Figure 3. sGluA2 levels predict spine fate. (*a*) A representative image of a dendritic branch with spines assigned to 1 of 4 groups based on increasing percentile rank of sGluA2 intensity. scale: 2.5 μm. (*b*) The fraction of stable spines (dark bars) and eliminated spines (light bars) was plotted per sGluA2 level groups in the WT and KO mice. For stable WT spines, 1: 0.38 ± 0.04, 2: 0.76 ± 0.018, 3: 0.92 ± 0.03 and 4: 1 ± 0, n = 4 mice. For stable KO spines, 1: 0.33 ± 0.05, 2: 0.59 ± 0.04, 3: 0.74 ± 0.03, and 4:0.95 ± 0.01, *n* = 5 mice. Repeated ANOVA analysis, *P < 0.5, **P < 0.01, ***P < 0.001. (*c*) sGluA2 spine rank within a local cluster determines spine fate. Top: A dendrite containing 2 clusters centered around spines with similar sGluA2 levels but opposing fates. Scale bar: 10 μm. Below: Magnified images of boxed areas. Numbers represent ranking of spines within a cluster, a 10 μm stretch centered around the target spine (dotted orange circle). The target spines had similar sGluA2 intensity but opposing fates. Note that their local ranking was different with the higher rank spine (right) persisting 48 h later while the spine with the lower rank (left) disappearing. Scale bar: 2.5 μm. (*d*) Mean local rank of similar sGluA2 containing spines was significantly higher in stable spines in both genotypes (WT: eliminated spines: 2.95 ± 0.36, stable spines: 5.66 ± 0.57, *n* = 34 spines; *n* = 30 spines, KO: eliminated spines: 3.46 ± 0.37, stable spines: 5.9 ± 0.39, *n* = 28 spines, *n* = 28 spines, Two-way ANOVA, ***P < 0.001). All data represented as mean ± SEM.

significantly larger increases over 10 days as compared to larger spines.

sGluA2 in Newly Formed and Eliminated Spines

Finally, we characterized AMPAR and spine relationship in newly formed and eliminated spine populations in the WT and KO mice. First to characterize newly formed spines, we followed spines formed within the first 40 h of the experiment (Fig. 5*a*–*c*, see Figure S5b for proportion of spines imaged at different imaging intervals) Although the fmr1 KO has increased rate of new spine formation (Fig. 2*b*), the overall stability of the newly formed structures was similar between the WT and the KO (Figure S5a). As expected soon after formation, the majority of newly formed spines were small and occupied the lowest ranks within their dendrites in both WT and KO (Figure S5b). Unlike in the preexisting spine population (Fig. 3*b*), spine stability of newly formed spines did not change with increasing initial levels of sGluA2 in either genotype (Figure S5c), suggesting that a certain threshold level of sGluA2 has to be reached for it to be a determinant of spine stabilization. Within 16–24 h after formation, sGluA2 levels increased by 49% and 43% in WT and KO respectively and continued to increase to 109% in WT ($P = 0.02$) and 91% in KO ($P = 0.04$) by 200 h post formation. We did not observe a difference between the genotypes in sGluA2 accumulation in newly formed spines (Fig. 5*a*–*c*). Although the size of the spines also increased by about 40% in both WT and KO after 200 h, these changes did not reach significance (Fig. 5*c*). Thus, newly formed spines are small and have low levels of sGluA2 soon after formation. Additionally, there is a gradual increase of AMPAR in both WT and KO with sGluA2 increases outpacing the spine size changes.

Lastly, to study eliminated spines, we pooled changes in sGluA2 and spine intensity of structures eliminated between 40

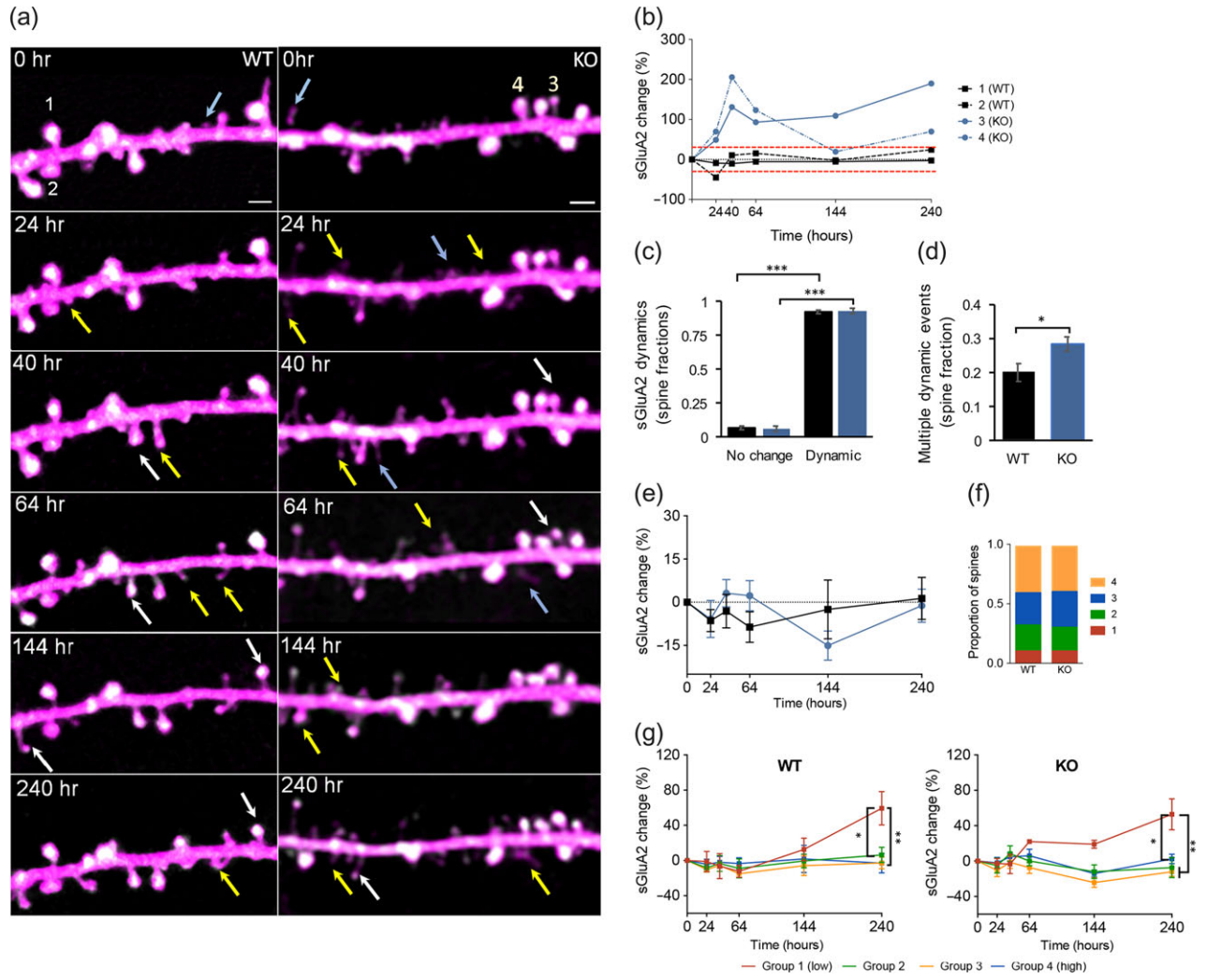

Figure 4. sGluA2 is dynamic within stable spines. (*a*) Representative time-lapse images (yellow arrows: new spines, blue arrows: eliminated spines, white arrows: spines with fluctuations in sGluA2). Scale bar: 2 µm. (*b*) sGluA2 intensity traces of marked spines in (*a*). Red dotted lines indicate cutoffs used for grouping (±30%). (*c*) Fraction of spines belonging to dynamic and no change groups in WT (black) and KO (blue) mice. The fraction of "No change" was significantly smaller than "dynamic" group (WT: No change: 0.07 ± 0.01, dynamic change: 0.93 ± 0.01, $n = 5$ mice, $P < 0.001$, KO: no change 0.07 ± 0.02, dynamic change: 0.93 ± 0.02, $n = 5$ mice, two-way ANOVA with Bonferroni correction,***$P < 0.001$). (*d*) Fraction of spines displaying multiple changes in direction of sGluA2 dynamics was significantly higher in KO (blue) compared to WT (black) (WT: 0.20 ± 0.02, KO: 0.28 ± 0.02, $n = 5$ mice, unpaired *t*-tests, $P = 0.04$). (*e*) Geometric mean of percentage change of sGluA2 intensity in stable spines across all imaging session. No difference was observed across time and genotypes ($n = 5$ mice, two-way repeated measure ANOVA with Bonferroni correction). (*f*) Proportion of stable spines classified according to varying sGluA2 levels at 0 h (Groups 1 to 4 have progressively increasing sGluA2 levels). The number of spines in each group is not equal since the classification into groups was performed at 0 h irrespective of future fate and smaller spines tend to be eliminated more. (*g*) Group 1 geometric mean of sGluA2 percent change at 240 h in both genotype was significantly higher than all other spine groups (WT 240 hours, Group 1: 59.4 ± 18%, Group 2: 6.4 ± 7%, Group 3: −3 ± 6%, Group 4: −3 ± 12.7%, KO 240 hours: Group 1: 52 ± 17%, Group 2: −7 ± 11%, Group 3: −12 ± 5%, Group 4: −2 ± 5%, $n = 5$ mice, one-way ANOVA with Bonferroni correction, *$P < 0.5$, **$P < 0.01$). Data presented as mean ± SEM.

and 64 h of the experiment (Fig. 6*a–d*). We observed a significant decrease (Fig. 6*b,d*) in sGluA2 (–28%, $P < 0.001$) and spine intensity (–17%, $P < 0.001$ in WT mice in the imaging session prior to elimination (16–24 h) that was not observed in the stable spines of the same dendrites (Fig. 6*c*). Interestingly, for both sGluA2 (–38%, $P < 0.001$) and spine intensity (–38.4%, $P < 0.001$), the decreases were significantly sharper in the KO ($P = 0.02$, $P < 0.001$, respectively) suggesting that the spine complex was being disassembled more rapidly in the KO. Although our study was not designed to determine the effects of circadian rhythm and sleep on GluA2 levels, we determined that a similar proportion of spines were imaged over evening–morning and morning–morning sessions in each genotype (Figure S6a) excluding the possibility that enhanced sGluA2 loss in the KO was due to overrepresentation of spines imaged at a certain time of day. Thus, we conclude that in both WT and KO spines shrink and loose AMPAR before elimination and this decrease is steeper in the fmr1 KO spines.

Discussion

Here, we report the first in vivo study that quantified changes in AMPAR in dendritic spines over multiple days. Using this approach, we characterized the relationship between AMPAR and spine stability in layer 2/3 pyramidal neurons in both WT and fmr1 KO mice. We found that sGluA2 levels within spines correlated with synaptic fate, with the largest spines being extremely stable (Fig. 3*a,b*). Consistent with this correlation,

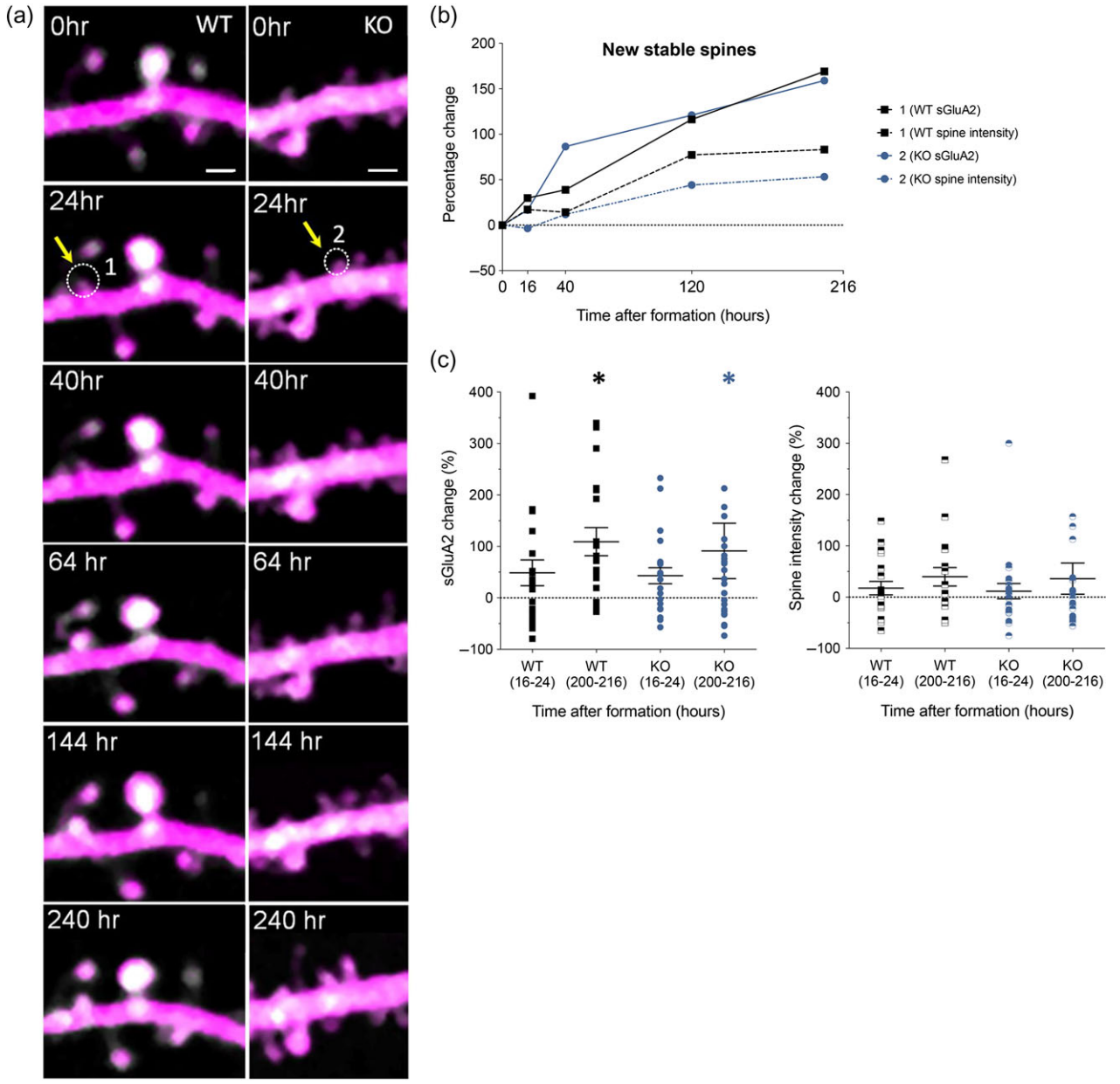

Figure 5. Newly formed spines gradually accumulated sGluA2 over time. (*a*) Representative time-lapse 2PLSM images showing formation of new spine from WT and KO (marked in white dotted circle) in WT (spine 1) and KO (spine 2) with corresponding sGluA2 and spine intensity traces shown in (*b*). Scale bar: 1.5 μm. (*c*) sGluA2 and spine intensity changes in stable new spines (WT sGluA2: 16–24 h 48.71 ± 25.21%, 200–216 h 109 ± 27.31%, $n = 19$ spines, KO sGluA2: 16–24 h 43.19 ± 15.58%, 200–216 h 91.23 ± 53.81%, $n = 22$ spines, Two-way ANOVA with Bonferroni correction, $^*P < 0.5$). Spine intensity change was not significant over time or across genotype (two-way ANOVA with Bonferroni correction). Data presented as mean ± SEM.

before elimination spines both shrunk in size and lost sGluA2 (Fig. 6) whereas stable new spines gradually accumulated sGluA2 (Fig. 5). sGluA2 content within persistent spines was dynamic (Fig. 4*a*–*c*) with majority of spines showing at least one dynamic event during the 10 days imaging period. Imaging of sGluA2 in spines of the fmr1 KO mice revealed several deficits. Dendritic spines in the KO were smaller (Fig. 2*e*), denser (Fig. 2*a*), and more dynamic (Fig. 2*b*–*d*) as well as had reduced sGluA2 to spine size correlation (Fig. 2*g*). In the KO, a greater proportion of spines exhibited more dynamic behaviors (Fig. 4*d*). Finally, before elimination, spines in the KO shrunk and lost sGluA2 faster as compared to the WT (Fig. 6*d*). In summary, we find that while levels of AMPAR within spines are dynamic, they are predictive of spine fates. Moreover, loss of FMRP impacts sGluA2 content in spines, thus affecting their dynamics.

AMPAR and Spine Dynamics

AMPAR are glutamate-gated cation channels that regulate majority of fast synaptic transmission in the brain (Anggono and Huganir 2012). AMPAR's are heteromeric tetramers composed of multiple subunits GluA1-4 (Anggono and Huganir 2012). Since majority of AMPAR are of GluA1–GluA2 heteromers (Lu et al. 2009), sGluA2 within spines is a good measure of functional synaptic AMPAR content (Makino and Malinow 2011;

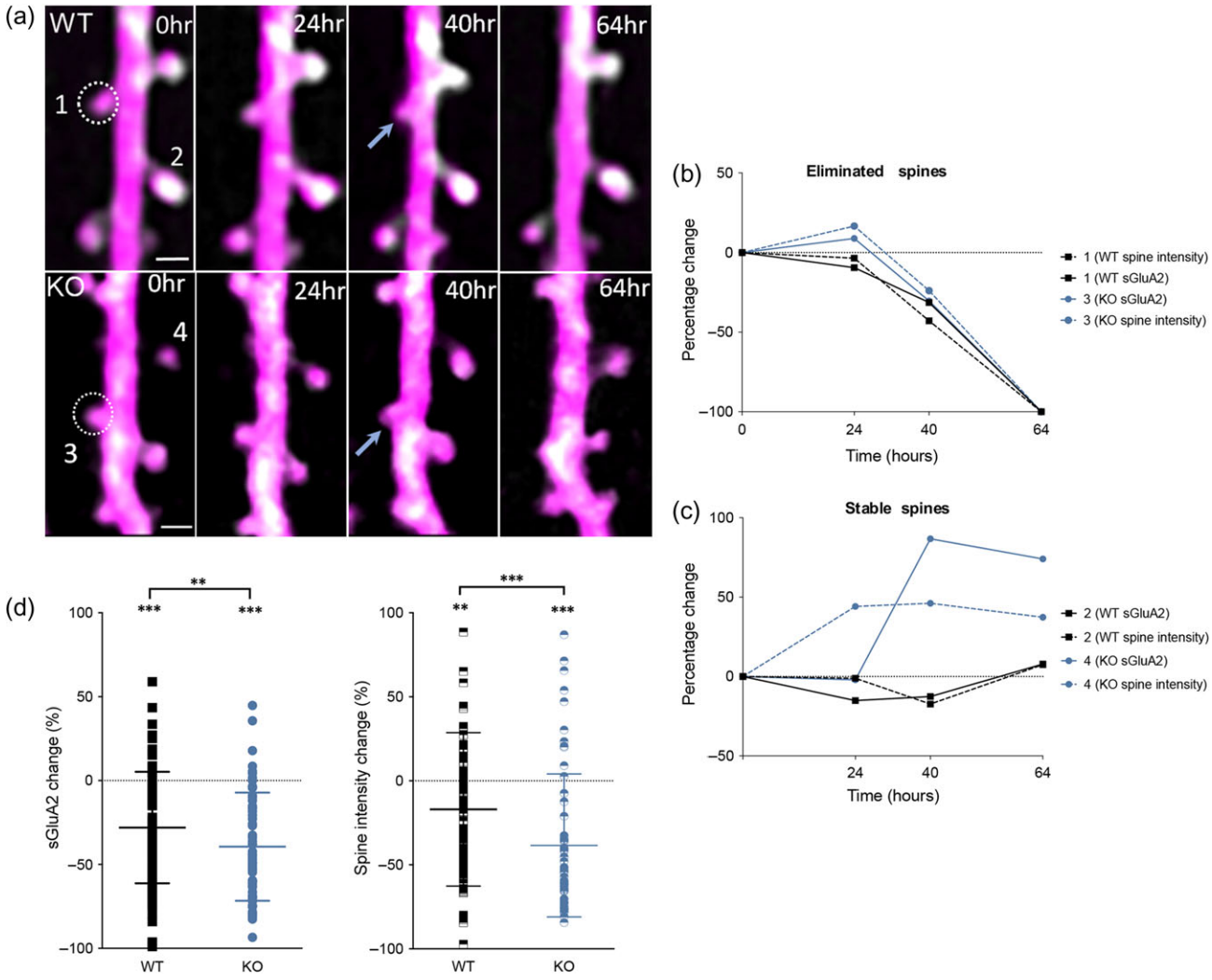

Figure 6. Eliminated spines have decrease in sGluA2 immediately before elimination. (*a*) Representative images of eliminated spines (1 and 3, circled) in WT and KO mice. Scale bar: 1 µm. (*b*) Individual traces of sGluA2 and spine intensity of eliminated spines 1 and 3. Note the gradual loss of sGluA2 and spine size shrinkage before elimination in both genotypes. (*c*) Stable spine 2 shows relatively little change in sGluA2 or spine intensity while spine 4 shows an increase in both sGluA2 and spine intensity. (*d*) Change in sGluA2 and spine intensity of eliminated spines 16–24 h prior to elimination (WT sGluA2: −28.01 ± 3.46%, KO sGluA2: −39.1 ± 4.19%, WT spine intensity: −16.94 ± 4.6%, KO spine intensity: −38.4 ± 5.53%, WT $n = 91$ spines, KO $n = 60$ spines, two-way ANOVA with Bonferroni correction, $^{*}P < 0.5$, $^{**}P < 0.01$, $^{***}P < 0.001$). Data presented as mean ± SEM.

Zhang et al. 2015). As long-term dynamic correlation between AMPAR and spine behavior has not been previously investigated in vivo, this was the primary goal of the study. Overexpression of sGluA2 construct in vivo did not alter synaptic properties such as density and TORs (Ma et al. 2016) in apical dendrites of Layer 2/3 pyramidal neurons (Figure S2d, Fig. 2*b–d*). Similarly, as expected from a postsynaptic protein sGluA2 expression was punctate and expressed primarily in dendrites with substantial localization in dendritic spines and no expression in axonal boutons (Figure S2a). Lack of aberrant expression of sGluA2, suggests that synaptic incorporation of AMPAR is a tightly regulated process (Kessels et al. 2009). All spines imaged in the study, including thin filopodial looking spines expressed some amount of sGluA2 (Figure S2b), suggesting that silent synapses may not be present in dendrites at this age. Since we did not observe a significant difference in the levels of tdTomato expression between the genotypes it is reasonable to assume that levels of sGluA2 overexpression are also similar. Nevertheless, our study cannot exclude the possibility that the composition of GluA subunits and regulation by activity is different in the KO.

Levels of synaptic AMPAR determine the strength of a synapse (Matsuzaki et al. 2001) and have been associated with synaptic stability (Grutzendler et al. 2002; Trachtenberg et al. 2002; Holtmaat et al. 2005). Consistent with this, we observe progressive stability of spines with increasing AMPAR levels (Fig. 3*b*). Large spines with highest levels of AMPAR were almost always persistent over 240 h whereas spines with least AMPAR had only 38% stability (Fig. 3*a,b*). Furthermore, we observed in both WT and KO mice relative AMPAR level of a spine within its local dendritic spine cluster correlated with synaptic stability. Similar sGluA2 containing spines were more likely to be stabilized when surrounded by lower versus higher sGluA2 containing spines (Fig. 3*c, d*). Unlike previous in vitro studies that linked neighboring synapse activity with synaptic fate (Fonseca et al. 2004; Oh et al. 2015), here we observed how local rank

based on synaptic AMPAR content alone correlates with spine fate. This suggests a potential competition between synapses for local stabilizing factors and likely involves similar biochemical signaling molecules and pathways regulating spatial organization of local dendritic microcircuits (Nishiyama and Yasuda 2015). We also observed spines hours prior to elimination to both lose AMPAR and shrink (Fig. 6*a–d*). This is consistent with results of activity-dependent structural plasticity where induction of LTD in slices resulted in shrinkage and even elimination of spines (Fonseca et al. 2004; Zhou et al. 2004; Bastrikova et al. 2008). In contrast, new spines which survived over many days gradually accumulated AMPAR to about 100% over 200 h (Fig. 5*a–c*). Surprisingly, spine size did not keep up with AMPAR changes and only increased by 40% (Fig. 5*c*). This breakdown in AMPAR and spine size correlation is in contrast to in vitro studies where spine size increases usually precede AMPAR increases (Kopec et al. 2007), suggesting a difference in spine behavior in vivo. Supporting this observation, in a recent in vivo study using whisker stimulation to stimulate spines, there was a similar increase in sGluA1 but not of spine size (Zhang et al. 2015). Nevertheless, as a population, persistent spine size and sGluA2 levels did not change over time in basal conditions. However, we did observe that small persistent spines gradually accumulated sGluA2 by 240 h. These small spines could have been recently formed spines which had similar sGluA2 profiles as newly formed spines. Lastly, we also observed AMPAR levels to be dynamic over days (Fig. 4*c*). Almost 90% of spines showed a 30% increase or decrease of AMPAR over time (Fig. 4*c*) with nearly 20% of spines showing multiple bidirectional sGluA2 changes (Fig. 4*d*). Although surprising since decreases in synaptic strength is thought to be detrimental to spine fate, this result is consistent with more recent in vivo studies where variable synaptic properties were observed even in stable spine populations (Cane et al. 2014; Villa et al. 2016; Diering et al. 2017). Also since many persistent spines show large decreases in sGluA2 (Fig. 4*a,b*) but still do not get eliminated, it might suggest that it's not the net decrease that determines spine fate but rather a threshold level beneath which a spine is eliminated.

Fragile X Spine and AMPAR Dynamics

Synaptic deficits in patients with FXS have been described with presence of dense dendrites and long immature spines (Irwin et al. 2000). Spine deficits in Fmr1 KO mice, an animal model of FXS, have varied depending on brain region, age and population of neurons investigated (He and Portera-Cailliau 2013). In this study, we observed in layer 2/3 pyramidal neurons of the primary motor cortex higher TORs (Fig. 2*b–d*), increased spine density (Fig. 2*a*) and smaller spines (Fig. 2*e*) in the KO. High TORs in the KO have been described previously in several in vivo studies (Cruz-Martin et al. 2010; Pan et al. 2010; Padmashri et al. 2013; Nagaoka et al. 2016) at different ages and population of neurons and our results are consistent with these findings. Reports of higher spine densities in the KO (Irwin et al. 2001; Dolen et al. 2007; Hodges et al. 2016), however, are more variable. In this study, we find a small (11%) but significant increase in spine density (Fig. 2*a*). Moreover, since spine formation is higher than elimination in these population of neurons (Formation 40% vs. Elimination 37% over 10 days), it would be expected to observe higher density. We also observed a significant population of small spines in the KO mice (Fig. 2*e*). Smaller spines in the KO are reminiscent of the human studies (Rudelli et al. 1985; Hinton et al. 1991; Irwin et al. 2001) and thought to represent a more immature phenotype of spines. Smaller spines are also more dynamic (Fig. 3*b*) and this supports our data of higher TOR in the KO. Unexpectedly, spine-AMPAR correlation was altered in the KO with less AMPAR per spine (Fig. 2*g*). Previous studies in the KO have not identified deficits in synaptic AMPAR content or function under basal conditions in the cortex (Gocel and Larson 2012; Padmashri et al. 2013; Martin et al. 2016), although reduced AMPAR have been observed in the amygdala (Suvrathan et al. 2010). Since, our study focused on specific subpopulation of synapses in apical dendrites of layer 2/3 neurons, these may represent a previously unappreciated deficit in the KO mouse and further studies are required.

Similar to the WT, spine stability increased with increasing sGluA2 content in the KO (Fig. 3*b*) with spines with the least and the most sGluA2 having similar stability to the WT. Additionally, correcting for the larger population of small spines in the KO by using WT sGluA2 intensity values as cut-offs, gave similar stability across all 4 spine groups (Figure S3a, b). Consistent with this result, KO spine stability was correlated with relative AMPAR levels within the local synaptic clusters (Fig. 3*d*) similar to the WT, thus overall suggesting no deficits to AMPAR and spine stability in the KO. Interestingly, the KO mice had exaggerated decreases in both AMPAR and spine sizes before elimination (Fig. 6*d*). Exaggerated internalization of AMPAR through elevated LTD (Huber et al. 2002; Bear et al. 2004) has been described in the KO and since LTD has been linked to synapse elimination (Nagerl et al. 2004; Bastrikova et al. 2008) it may explain the enhanced elimination in the KO. Finally, it is important to point out that most elimination events described in vitro were on the time scale of minutes whereas in this study changes over hours are observed suggesting protracted AMPAR decreases before elimination in vivo.

Unlike elimination, newly formed spines in the KO had similar stability, as well as AMPAR and spine changes (Fig. 5*a–d*) as the WT, suggesting loss of FMRP does not affect growth and stabilization of synapses. This is consistent with previous studies that demonstrate that stability of new spines formed following experience is unaffected in the KO (Pan et al. 2010; Reiner and Dunaevsky 2015). Interestingly, a larger percentage of KO spines showed more dynamic events over days (Fig. 4*d*) suggesting less stable synaptic strength in KO which further could impact the function of neuronal circuits in FXS.

Supplementary Material

Supplementary data are available at *Cerebral Cortex* online.

Funding

This work was supported by National Institute of Child Health and Human Development R01 grant HD67218 (A.D.), by National Institute of Mental Health R21 grant MH107029 (A.D.), and by an American Heart Association Predoctoral Fellowship 15PRE23280027 (A.S).

Notes

We would like to thank Florent Mayé for developing the neuron analyzer package, Robin High for the statistics, Yoosun Jung for maintaining the animal colony and assistance with the overexpression analysis, Channabasavaiah Gurumurthy and Rolen Quadros Mackey for cloning the pCAG-Td Tom construct, Bina Ranjith for help with the analysis and Padmashri Ragunathan

for discussion and critical input on the manuscript. *Conflict of Interest*: None declared.

References

Alvarez VA, Sabatini BL. 2007. Anatomical and physiological plasticity of dendritic spines. Annu Rev Neurosci. 30:79–97.

Anggono V, Huganir RL. 2012. Regulation of AMPA receptor trafficking and synaptic plasticity. Curr Opin Neurobiol. 223: 461–469.

Bastrikova N, Gardner GA, Reece JM, Jeromin A, Dudek SM. 2008. Synapse elimination accompanies functional plasticity in hippocampal neurons. Proc Natl Acad Sci USA. 1058: 3123–3127.

Bear MF, Huber KM, Warren ST. 2004. The mGluR theory of fragile X mental retardation. Trends Neurosci. 277:370–377.

Bosch M, Hayashi Y. 2012. Structural plasticity of dendritic spines. Curr Opin Neurobiol. 223:383–388.

Cajal SR. 1888. Estructura de los centros nerviosos de las aves. Rev Trim Histol Norm Pat. 1:1–10.

Cane M, Maco B, Knott G, Holtmaat A. 2014. The relationship between PSD-95 clustering and spine stability in vivo. J Neurosci. 346:2075–2086.

Chater TE, Goda Y. 2014. The role of AMPA receptors in postsynaptic mechanisms of synaptic plasticity. Front Cell Neurosci. 8:401.

Contractor A, Klyachko VA, Portera-Cailliau C. 2015. Altered neuronal and circuit excitability in fragile X syndrome. Neuron. 874:699–715.

Cruz-Martin A, Crespo M, Portera-Cailliau C. 2010. Delayed stabilization of dendritic spines in fragile X mice. J Neurosci. 3023:7793–7803.

Diering GH, Nirujogi RS, Roth RH, Worley PF, Pandey A, Huganir RL. 2017. Homer1a drives homeostatic scaling-down of excitatory synapses during sleep. Science. 3556324:511–515.

Dolen G, Osterweil E, Rao BS, Smith GB, Auerbach BD, Chattarji S, Bear MF. 2007. Correction of fragile X syndrome in mice. Neuron. 566:955–962.

Dunaevsky A, Tashiro A, Majewska A, Mason C, Yuste R. 1999. Developmental regulation of spine motility in the mammalian central nervous system. Proc Natl Acad Sci USA. 96: 13438–13443.

Engert F, Bonhoeffer T. 1999. Dendritic spine changes associated with hippocampal long-term synaptic plasticity. Nature. 3996731:66–70.

Fonseca R, Nagerl UV, Bonhoeffer T. 2006. Neuronal activity determines the protein synthesis dependence of long-term potentiation. Nat Neurosci. 94:478–480.

Fonseca R, Nagerl UV, Morris RG, Bonhoeffer T. 2004. Competing for memory: hippocampal LTP under regimes of reduced protein synthesis. Neuron. 446:1011–1020.

Fu M, Zuo Y. 2011. Experience-dependent structural plasticity in the cortex. Trends Neurosci. 344:177–187.

Gocel J, Larson J. 2012. Synaptic NMDA receptor-mediated currents in anterior piriform cortex are reduced in the adult fragile X mouse. Neuroscience. 221:170–181.

Gray EG. 1959. Axo-somatic and axo-dendritic synapses of the cerebral cortex: an electron microscopic study. J Anat. 83: 420–433.

Grutzendler J, Kasthuri N, Gan WB. 2002. Long-term dendritic spine stability in the adult cortex. Nature. 4206917:812–816.

Hasegawa S, Sakuragi S, Tominaga-Yoshino K, Ogura A. 2015. Dendritic spine dynamics leading to spine elimination after repeated inductions of LTD. Sci Rep. 5:7707.

Hayashi-Takagi A, Yagishita S, Nakamura M, Shirai F, Wu YI, Loshbaugh AL, Kuhlman B, Hahn KM, Kasai H. 2015. Labelling and optical erasure of synaptic memory traces in the motor cortex. Nature. 5257569:333–338.

He CX, Portera-Cailliau C. 2013. The trouble with spines in fragile X syndrome: density, maturity and plasticity. Neuroscience. 251:120–128.

Hinton VJ, Brown WT, Wisniewski K, Rudelli RD. 1991. Analysis of neocortex in three males with the fragile X syndrome. Am J Med Genet. 41:289–294.

Hodges JL, Yu X, Gilmore A, Bennett H, Tjia M, Perna JF, Chen CC, Li X, Lu J, Zuo Y. 2016. Astrocytic contributions to synaptic and learning abnormalities in a mouse model of fragile X syndrome. Biol Psychiatry. S0006-3223(16):32779–32772.

Hofer SB, Bonhoeffer T. 2010. Dendritic spines: the stuff that memories are made of? Curr Biol. 204:R157–R159.

Holtmaat A, Bonhoeffer T, Chow DK, Chuckowree J, De Paola V, Hofer SB, Hubener M, Keck T, Knott G, Lee WC, et al. 2009. Long-term, high-resolution imaging in the mouse neocortex through a chronic cranial window. Nat Protoc. 48:1128–1144.

Holtmaat A, Svoboda K. 2009. Experience-dependent structural synaptic plasticity in the mammalian brain. Nat Rev Neurosci. 109:647–658.

Holtmaat AJ, Trachtenberg JT, Wilbrecht L, Shepherd GM, Zhang X, Knott GW, Svoboda K. 2005. Transient and persistent dendritic spines in the neocortex in vivo. Neuron. 452: 279–291.

Huber KM, Gallagher SM, Warren ST, Bear MF. 2002. Altered synaptic plasticity in a mouse model of fragile X mental retardation. Proc Natl Acad Sci USA. 9911:7746–7750.

Irwin SA, Galvez R, Greenough WT. 2000. Dendritic spine structural anomalies in fragile-X mental retardation syndrome. Cereb Cortex. 10:1038–1044.

Irwin SA, Patel B, Idupulapati M, Harris JB, Crisostomo RA, Larsen BP, Kooy F, Willems PJ, Cras P, Kozlowski PB, et al. 2001. Abnormal dendritic spine characteristics in the temporal and visual cortices of patients with fragile-X syndrome: a quantitative examination. Am J Med Genet. 982:161–167.

Kessels HW, Kopec CD, Klein ME, Malinow R. 2009. Roles of stargazin and phosphorylation in the control of AMPA receptor subcellular distribution. Nat Neurosci. 127:888–896.

Kopec CD, Li B, Wei W, Boehm J, Malinow R. 2006. Glutamate receptor exocytosis and spine enlargement during chemically induced long-term potentiation. J Neurosci. 267: 2000–2009.

Kopec CD, Real E, Kessels HW, Malinow R. 2007. GluR1 links structural and functional plasticity at excitatory synapses. J Neurosci. 2750:13706–13718.

Lu W, Shi Y, Jackson AC, Bjorgan K, During MJ, Sprengel R, Seeburg PH, Nicoll RA. 2009. Subunit composition of synaptic AMPA receptors revealed by a single-cell genetic approach. Neuron. 622:254–268.

Ma L, Qiao Q, Tsai JW, Yang G, Li W, Gan WB. 2016. Experience-dependent plasticity of dendritic spines of layer 2/3 pyramidal neurons in the mouse cortex. Dev Neurobiol. 763:277–286.

Makino H, Malinow R. 2011. Compartmentalized versus global synaptic plasticity on dendrites controlled by experience. Neuron. 726:1001–1011.

Malenka RC, Bear MF. 2004. LTP and LTD: an embarrassment of riches. Neuron. 441:5–21.

Martin HG, Lassalle O, Brown JT, Manzoni OJ. 2016. Age-dependent long-term potentiation deficits in the prefrontal cortex of the Fmr1 knockout mouse model of fragile X syndrome. Cereb Cortex. 265:2084–2092.

Matsuzaki M, Ellis-Davies GC, Nemoto T, Miyashita Y, Iino M, Kasai H. 2001. Dendritic spine geometry is critical for AMPA receptor expression in hippocampal CA1 pyramidal neurons. Nat Neurosci. 411:1086–1092.

Matsuzaki M, Honkura N, Ellis-Davies GC, Kasai H. 2004. Structural basis of long-term potentiation in single dendritic spines. Nature. 4296993:761–766.

Miesenbock G, De Angelis DA, Rothman JE. 1998. Visualizing secretion and synaptic transmission with pH-sensitive green fluorescent proteins. Nature. 3946689:192–195.

Nagaoka A, Takehara H, Hayashi-Takagi A, Noguchi J, Ishii K, Shirai F, Yagishita S, Akagi T, Ichiki T, Kasai H. 2016. Abnormal intrinsic dynamics of dendritic spines in a fragile X syndrome mouse model in vivo. Sci Rep. 6:26651.

Nagerl UV, Eberhorn N, Cambridge SB, Bonhoeffer T. 2004. Bidirectional activity-dependent morphological plasticity in hippocampal neurons. Neuron. 445:759–767.

Nishiyama J, Yasuda R. 2015. Biochemical computation for spine structural plasticity. Neuron. 871:63–75.

Noguchi J, Nagaoka A, Watanabe S, Ellis-Davies GC, Kitamura K, Kano M, Matsuzaki M, Kasai H. 2011. In vivo two-photon uncaging of glutamate revealing the structure-function relationships of dendritic spines in the neocortex of adult mice. J Physiol. 589Pt 10:2447–2457.

Oh WC, Parajuli LK, Zito K. 2015. Heterosynaptic structural plasticity on local dendritic segments of hippocampal CA1 neurons. Cell Rep. 102:162–169.

Padmashri R, Reiner BC, Suresh A, Spartz E, Dunaevsky A. 2013. Altered structural and functional synaptic plasticity with motor skill learning in a mouse model of fragile x syndrome. J Neurosci. 3350:19715–19723.

Pan F, Aldridge GM, Greenough WT, Gan WB. 2010. Dendritic spine instability and insensitivity to modulation by sensory experience in a mouse model of fragile X syndrome. Proc Natl Acad Sci USA. 10741:17768–17773.

Penagarikano O, Mulle JG, Warren ST. 2007. The pathophysiology of fragile x syndrome. Annu Rev Genomics Hum Genet. 8:109–129.

Penzes P, Cahill ME, Jones KA, VanLeeuwen JE, Woolfrey KM. 2011. Dendritic spine pathology in neuropsychiatric disorders. Nat Neurosci. 143:285–293.

Pologruto TA, Sabatini BL, Svoboda K. 2003. ScanImage: flexible software for operating laser scanning microscopes. Biomed Eng Online. 2:13.

Reiner BC, Dunaevsky A. 2015. Deficit in motor training-induced clustering, but not stabilization, of new dendritic spines in fmr1 knock-out mice. PLoS One. 105:e0126572.

Rudelli RD, Brown WT, Wisniewski K, Jenkins EC, Laure-Kamionowska M, Connel W, Wisniewski HM. 1985. Adult fragile X syndrome cliniconeuropathologic findings. Acta Neuropathol. 67:289–295.

Saito T, Nakatsuji N. 2001. Efficient gene transfer into the embryonic mouse brain using in vivo electroporation. Dev Biol. 2401:237–246.

Suvrathan A, Hoeffer CA, Wong H, Klann E, Chattarji S. 2010. Characterization and reversal of synaptic defects in the amygdala in a mouse model of fragile X syndrome. Proc Natl Acad Sci USA. 10725:11591–11596.

Tennant KA, Adkins DL, Donlan NA, Asay AL, Thomas N, Kleim JA, Jones TA. 2011. The organization of the forelimb representation of the C57BL/6 mouse motor cortex as defined by intracortical microstimulation and cytoarchitecture. Cereb Cortex. 21(4):865–876.

Trachtenberg JT, Chen BE, Knott GW, Feng G, Sanes JR, Welker E, Svoboda K. 2002. Long-term in vivo imaging of experience-dependent synaptic plasticity in adult cortex. Nature. 4206917:788–794.

Turrigiano G. 2012. Homeostatic synaptic plasticity: local and global mechanisms for stabilizing neuronal function. Cold Spring Harb Perspect Biol. 41:a005736.

Villa KL, Berry KP, Subramanian J, Cha JW, Oh WC, Kwon HB, Kubota Y, So PT, Nedivi E. 2016. Inhibitory synapses are repeatedly assembled and removed at persistent sites in vivo. Neuron. 894:756–769.

Zeidan A, Ziv NE. 2012. Neuroligin-1 loss is associated with reduced tenacity of excitatory synapses. PLoS One. 77: e42314.

Zhang Y, Cudmore RH, Lin DT, Linden DJ, Huganir RL. 2015. Visualization of NMDA receptor-dependent AMPA receptor synaptic plasticity in vivo. Nat Neurosci. 183: 402–407.

Zhou Q, Homma KJ, Poo MM. 2004. Shrinkage of dendritic spines associated with long-term depression of hippocampal synapses. Neuron. 445:749–757.

Zito K, Scheuss V, Knott G, Hill T, Svoboda K. 2009. Rapid functional maturation of nascent dendritic spines. Neuron. 612: 247–258.